

T-GMP: Terrain-conditioned Generative Motion Priors for Versatile and Natural Humanoid Locomotion

Junhong Guo^{1,2,*} Hao Hu^{1,*} Chen Chen¹ Haoxuan Han¹ Linao Gong¹
Xin Yang¹ Zhicheng He^{1,2} Yao Su² Fenghua He^{1,†}
¹ Harbin Institute of Technology
² Leju Robotics

* Equal contribution; order decided by coin toss. † Corresponding author.



Figure 1: We present T-GMP, a terrain-conditioned generative motion priors module that enables robots to exhibit versatile and natural behaviors across diverse terrains. Trained only once, the robot learns whole-body coordination strategies, including natural arm swinging during walking, lowering the center of mass (CoM) on stairs and slopes, and extending the arms for balance when crossing gaps or narrow beams. Videos are available on our project website: <https://t-gmp.github.io>.

Abstract: Achieving both anthropomorphic naturalness and robust terrain traversal remains a fundamental challenge in humanoid locomotion. Existing Reinforcement Learning (RL) approaches typically rely on fixed motion priors, limiting their adaptability to varying environments. We propose Terrain-conditioned Generative Motion Priors (T-GMP), a module that captures a terrain-conditioned latent motion manifold from a few expert state-terrain demonstrations using a Conditional Variational Autoencoder (CVAE). The learned priors enable smooth style transitions, facilitating a unified policy that adapts to terrain variations. We integrate T-GMP into an adversarial learning pipeline with our proposed Foothold Penalty, where a discriminator dynamically modulates naturalness constraints conditioned on local terrain features, guiding the generation of versatile and human-like motions. Experimental results demonstrate that our method outperforms existing baselines in traversal success rate and motion smoothness, while preserving biomimetically natural and physically coordinated motions.

Keywords: Generative Motion Priors, Adversarial Learning, Humanoid Robot.

1 Introduction

The pursuit of versatile and human-like locomotion in humanoid robots is a fundamental goal in robotics, bridging the gap between mechanical efficiency and biological elegance. While Reinforcement Learning (RL) has achieved remarkable success in enabling robots to locomote robustly [1, 2, 3, 4] and traverse challenging terrains [5, 6, 7, 8], the resulting motions often exhibit “robotic” artifacts—stiffness, unnatural joint configurations, or a lack of biological plausibility. This is primarily because hand-crafted reward functions are often insufficient to capture the nuanced dynamics of human balance, especially when the robot must simultaneously optimize task objectives (e.g., velocity tracking) and stylistic constraints across diverse terrains.

To improve motion quality, mimic-based approaches [9, 10, 11, 12] have been widely adopted to distill “naturalness” and “agility” from motion capture (MoCap) data into policies, enabling robots to demonstrate highly dynamic skills such as jumping, dancing, and backflipping. However, when a robot encounters complex terrains, fixed and terrain-agnostic motion priors penalize the necessary deviations required for physical stability. This creates a fundamental conflict between task completion and style preservation, often leading to stiff gaits or failure under varying environments.

To address these limitations, we propose T-GMP, a module designed for adaptive and anthropomorphic humanoid locomotion. Our core insight is that human motion is intrinsically linked to the environment; therefore, a motion prior should not be a static template but a dynamic manifold conditioned on terrain features. By utilizing a Conditional Variational Autoencoder (CVAE), T-GMP learns a terrain-conditioned latent motion manifold from a few expert state-terrain demonstrations. This enables the robot to learn how anthropomorphic motion styles adapt to different environments and achieve smooth style transitions across varying terrains.

Furthermore, we integrate T-GMP into a unified adversarial reinforcement learning framework, where the proposed terrain-conditioned discriminator injects terrain-aware anthropomorphic motion-style constraints into policy learning. To improve foothold stability on complex terrains, we further introduce a Foothold Penalty that explicitly regularizes foot-terrain contact quality, thereby enhancing locomotion robustness. Experimental results demonstrate that the proposed method generates coordinated and anthropomorphic whole-body behaviors across diverse terrains, while significantly outperforming baselines in traversal success rate and motion smoothness.

Overall, our contributions can be summarized as follows:

- 1) We propose T-GMP, a module that learns a terrain-conditioned latent motion manifold from a few expert state-terrain demonstrations, enabling the generation of terrain-adaptive motion priors.
- 2) By introducing a terrain-conditioned discriminator, we integrate T-GMP into a unified adversarial RL paradigm that jointly optimizes task objectives and motion style constraints.
- 3) We conduct full-size humanoid robot deployment experiments across eight terrains, demonstrating that the proposed method can generate diverse, coordinated, and anthropomorphic whole-body motions while outperforming baselines in traversal success rate and motion smoothness.

2 Related Works

Legged Locomotion Recent advancements in humanoid locomotion have seen a transition from proprioceptive-only methods to perception-aware approaches. While proprioceptive-only methods [13, 14, 15, 16, 17] demonstrate impressive robustness through proprioceptive feedback, they are limited by a reactive control loop that may cause hardware damage during abrupt terrain changes. Conversely, perception-aware policies utilize depth sensors [18, 19, 20, 21, 22, 23, 24, 25] or LiDAR [26, 27, 28, 29, 30, 31] to construct egocentric terrain representations and enable proactive maneuvers. However, existing perception-driven methods predominantly focus on lower-limb stability and gait scheduling, frequently overlooking the whole-body coordination potential inherent in the humanoid form. Our work addresses this gap by phrasing locomotion as a terrain-conditioned whole-body coordination task. By integrating perception with generative motion priors, our frame-

work enables the robot to autonomously recruit its entire skeletal structure, including arms and torso, to maintain stability over challenging obstacles.

Generative Motion Priors Leveraging human motion priors to enhance anthropomorphic locomotion has become a prevailing direction in recent robotics research. Mimic-based approaches [9, 32, 33] directly track human MoCap data, enabling robots to exhibit natural and versatile skills. However, such methods typically rely on fixed reference trajectories, which limit their ability to generalize to multi-terrain traversal scenarios with complex and varying conditions. To improve generalization, subsequent studies abstract human motion priors into transferable motion styles that guide policies to produce human-like behaviors [34, 35, 36, 10, 37, 38]. Although these methods partially alleviate the dependence on a single reference trajectory, the underlying motion priors are still fixed, making it difficult to adapt to diverse terrains. More recently, generative motion priors [39, 40, 41, 42] have been introduced to model richer motion distributions, enabling robots to exhibit natural motion styles and smooth style transitions. We further integrate generative motion priors with terrain perception, generating motion priors conditioned on local terrain features during the locomotion policy training process. Moreover, we employ a terrain-conditioned discriminator to distill the motion priors into the policy during training, enabling natural and smooth anthropomorphic locomotion across various terrains.

3 Terrain-conditioned Generative Motion Priors

3.1 Data Collection

To jointly model locomotion robustness and anthropomorphic naturalness over complex terrains, we construct a terrain-conditioned motion dataset by combining privileged policy data with human MoCap data. Specifically, privileged expert policies are used to generate physically feasible and terrain-adaptive robot motions, while MoCap data provide natural human motion priors.

On challenging terrains (e.g., *stairs*, *slope*, and *beam*), we train multiple privileged expert policies in parallel and subsequently use the learned policies to collect terrain-conditioned locomotion data on their corresponding terrains. Specifically, at each time step t , the expert state is recorded as:

$$s_t = [q_t, \dot{q}_t, p_t], \quad (1)$$

where q_t and \dot{q}_t denote joint positions and velocities, and p_t denotes end-effector positions relative to the root frame. In addition, the corresponding local height map h_t is collected simultaneously.

To introduce anthropomorphic motion priors, MoCap data are collected on terrains that are amenable to motion capture acquisition (e.g., *flat*, *gap*, and *stage*), thereby preserving natural whole-body coordination characteristics. The captured human motions are then retargeted via General Motion Retargeting (GMR) [43] into executable robot trajectories satisfying kinematic and dynamic constraints, while the corresponding height map sequences are synchronously generated in simulation.

Finally, we construct a high-quality expert dataset $\mathcal{D} = \mathcal{D}_{\text{priv}} \cup \mathcal{D}_{\text{mocap}}$ spanning diverse terrain-aware motion styles. For each trajectory $d \in \mathcal{D}$, $d = \{(s_t, h_t)\}_{t=1}^L$ denotes the expert dataset collected on a single terrain, where L denotes the trajectory length. Details regarding the privileged policy training are provided in Section A.

3.2 Terrain-conditioned Generative Motion Priors

We adopt a CVAE to model multi-style motion distributions, and use its decoder as T-GMP. To explicitly incorporate terrain-conditioned information, we employ a two-layer CNN f_{cnn}^c to extract features from the local height map h_t , yielding a terrain embedding $h_t^{\text{emb}, c} = f_{\text{cnn}}^c(h_t)$. Building on this representation, we extend the standard β -VAE [44] to a conditional β -VAE formulation. The CVAE decoder conditions on the terrain embedding $h_t^{\text{emb}, c}$, together with a latent variable z_t sampled from the prior distribution $p(z_t)$, generates expert state trajectory sequences, which exhibit

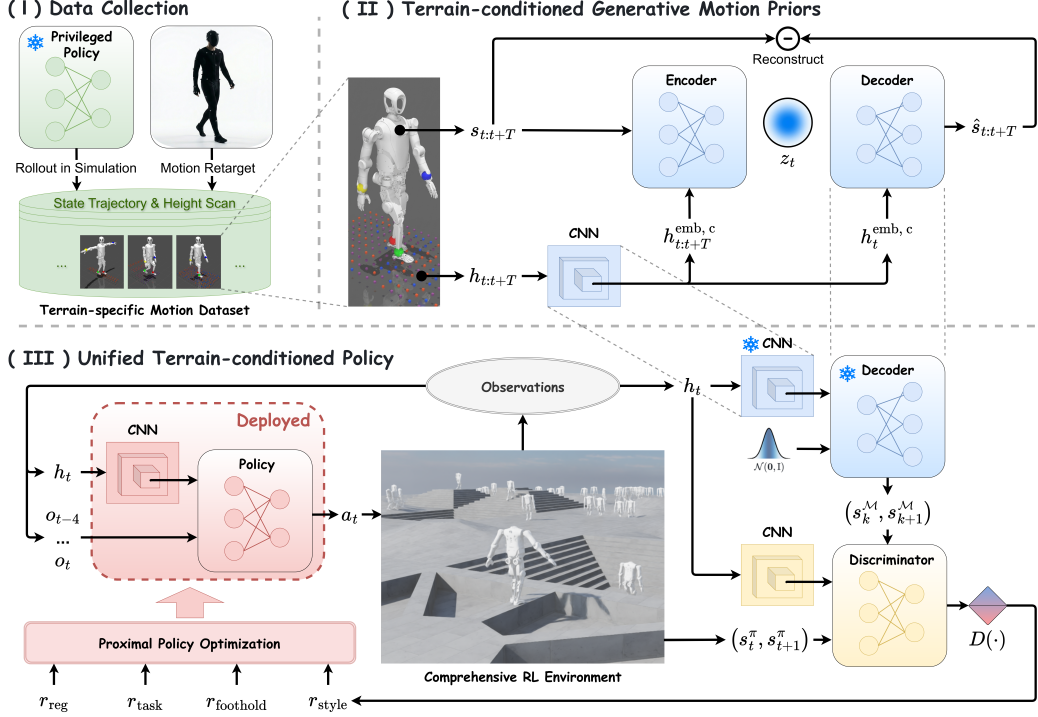


Figure 2: **Method Overview.** The overall learning pipeline consists of three parts: (I) collecting expert locomotion data using privileged expert policies and human motion capture, (II) training T-GMP using a CVAE, and (III) training a unified RL policy with a terrain-conditioned discriminator. The terrain representation (height map) serves as a conditioning variable across all modules.

diverse motion styles across different terrains:

$$\hat{s}_{t:t+T} = \text{Decoder}(z_t, h_t^{\text{emb}, c}). \quad (2)$$

The overall architecture of the CVAE is illustrated in Figure 2 (II). The model is trained by minimizing a weighted sum of a reconstruction loss and a regularization term, defined as:

$$\begin{aligned} \mathcal{L}_{\text{cvae}} = & \mathbb{E}_{(s_{t:t+T}, h_{t:t+T}) \sim \mathcal{D}} [\mathbb{E}_{q_\phi(z_t | s_{t:t+T}, h_{t:t+T}^{\text{emb}, c})} [\|s_{t:t+T} - \hat{s}_{t:t+T}\|_2^2] \\ & + \beta D_{\text{KL}}(q_\phi(z_t | s_{t:t+T}, h_{t:t+T}^{\text{emb}, c}) || p(z_t))], \end{aligned} \quad (3)$$

where $s_{t:t+T}$ and $h_{t:t+T}^{\text{emb}, c}$ respectively denote a sequence of T consecutive expert states and their corresponding local height map features, and β balances reconstruction accuracy and latent space regularization. We adopt a standard normal distribution $\mathcal{N}(0, I)$ as the prior distribution $p(z_t)$.

During real-world deployment, only the local height map observation at the current time step is available. Therefore, when reconstructing expert state trajectory sequences, we condition the decoder solely on a single-frame height map h_t to ensure consistency between training and inference. This design inevitably introduces a certain loss in reconstruction accuracy. To mitigate error accumulation caused by insufficient conditioning information, we shorten the reconstruction horizon T , thereby effectively limiting the propagation of long-horizon prediction errors. The entire CVAE is trained in an offline manner to fully leverage the previously constructed expert motion dataset.

4 Unified Terrain-conditioned Policy Training

4.1 Terrain-conditioned Discriminator

To enable the robot to exhibit natural, whole-body coordinated humanoid motion styles when traversing diverse terrains, we introduce adversarial motion priors (AMP) [34] to endow the pol-

icy with anthropomorphic style from the expert dataset. However, when multiple motion priors simultaneously cover the same task, the standard AMP framework may cause distinct motion styles to collapse into indistinguishable behaviors during policy learning. To address this problem, we extend the AMP discriminator to a terrain-conditioned discriminator. Specifically, we employ a five-layer CNN $f_{\text{cnn}}^{\text{d}}$ to extract terrain features from the local height map h_t , and use the resulting terrain embedding $h_t^{\text{emb, d}}$ as a conditioning input, together with state transitions, to guide the policy toward learning distinct and diverse motion styles under varying terrains.

During discriminator training, we use the decoder trained in Section 3.2 to generate expert state trajectory sequences $\tau_t^{\mathcal{M}} = [s_t^{\mathcal{M}}, \dots, s_{t+T}^{\mathcal{M}}]$ online conditioned on the terrain features, from which expert state transition pairs $(s_k^{\mathcal{M}}, s_{k+1}^{\mathcal{M}})$ are randomly sampled, where $t \leq k < t + T$. In parallel, policy-induced state transition pairs $(s_t^{\pi}, s_{t+1}^{\pi})$ are obtained from environment rollouts by executing the current policy, where s_t^{π} denotes the policy state at time step t and s_{t+1}^{π} denotes the resulting next state under the policy.

Unlike the formulation in AMP [34], our terrain-conditioned discriminator D is trained by minimizing the following objective:

$$\begin{aligned} \arg \min_D \quad & \mathbb{E}_{d^{\mathcal{M}}(s_k, s_{k+1})} [(D(s_k, s_{k+1} | h_t^{\text{emb, d}}) - 1)^2] \\ & + \mathbb{E}_{d^{\pi}(s_t, s_{t+1})} [(D(s_t, s_{t+1} | h_t^{\text{emb, d}}) + 1)^2] \\ & + \frac{\mathbf{w}^{\text{gp}}}{2} \mathbb{E}_{d^{\mathcal{M}}(s_k, s_{k+1})} [\|\nabla_{\phi} D(\phi)|_{\phi=(s_k, s_{k+1} | h_t^{\text{emb, d}})}\|^2], \end{aligned} \quad (4)$$

where $h_t^{\text{emb, d}}$ represents local height map features extracted by the five-layer CNN $f_{\text{cnn}}^{\text{d}}$, $d^{\mathcal{M}}$ and d^{π} respectively represent the decoder-generated expert state transition distribution and the policy-induced state transition distribution, and \mathbf{w}^{gp} is the weight of the gradient penalty term.

During policy training, to provide the policy with a clear and stable style guidance signal, we convert the discriminator output into a style reward, which is defined as:

$$r_{\text{amp}} = \max[0, 1 - (D(s_t^{\pi}, s_{t+1}^{\pi}) - 1)^2/4]. \quad (5)$$

This reward function encourages policy-induced state transitions to align with the terrain-conditioned expert motion styles, thereby guiding the policy to acquire consistent yet terrain-distinctive locomotion behaviors across diverse terrains.

4.2 Policy Training

Observations We define the robot’s observation at time step t as:

$$\mathbf{o}_t = [\omega_t, \mathbf{g}_t, q_t, \dot{q}_t, a_{t-1}], \quad (6)$$

where ω_t denotes the angular velocity of the robot’s root, \mathbf{g}_t is the gravity direction vector, q_t and \dot{q}_t respectively represent joint positions and velocities, and $a_{t-1} \in \mathbb{R}^{26}$ denotes the action executed at the previous time step. To enhance temporal awareness and robustness, we stack the most recent five frames of observations, forming an augmented observation $\mathbf{O}_t = [\mathbf{o}_{t-4}, \dots, \mathbf{o}_t]$. In addition, the Critic network has access to privileged information $\mathbf{o}_t^{\text{priv}}$ during training to improve the accuracy of value estimation. Detailed information about \mathbf{o}_t and $\mathbf{o}_t^{\text{priv}}$ are provided in Section B.1.

Policy The overall training framework is illustrated in Figure 2 (III). To enable the policy to exhibit discriminative motion styles while maintaining strong terrain adaptability across different terrains, we explicitly incorporate terrain perception into the policy network. Specifically, we employ a CNN $f_{\text{cnn}}^{\text{p}}$ with the same architecture described in Section 3.2 to extract features from the local height map h_t , and concatenate the resulting terrain embedding $h_t^{\text{emb, p}}$ with the robot’s augmented proprioceptive observation \mathbf{O}_t as input to the policy network. This design allows the policy to: (1) learn differentiated motion styles under varying terrains, and (2) attend to local terrain features, thereby perceiving terrain changes and guiding the robot to make more anticipatory decisions. Detailed policy training configurations and network architectures are provided in Section B.2.

Foothold Penalty During policy training, the robot may exhibit undesirable foothold behaviors when interacting with terrain edges and foothold contacts, such as kicking stair edges during ascent and edge-sliding during descent, which significantly degrade motion naturalness and physical plausibility. To address this problem, we introduce Foothold Penalty, which explicitly constrains foot-terrain contact quality through ray-cast distance measurements from the toe and sole regions. Specifically, the toe distance is used to penalize toe collisions:

$$r_{\text{toe}} = -\max(0, (\frac{d_{\text{toe}}^{\text{threshold}} - d_{\text{toe}}}{d_{\text{toe}}^{\text{threshold}}})^3), \quad (7)$$

where d_{toe} denotes the minimum distance between the toe and the terrain surface, $d_{\text{toe}}^{\text{threshold}}$ denotes the safety distance threshold. The sole distance suppresses edge-support and sliding behaviors:

$$r_{\text{sole}} = -\text{clip}(d_{\text{sole}} - d_{\text{sole}}^{\text{threshold}}, 0, 1) \cdot \mathbb{I}_{\text{contact}}, \quad (8)$$

where d_{sole} denotes the maximum distance between the sole and the ground surface, $d_{\text{sole}}^{\text{threshold}}$ denotes the maximum allowable support distance, and $\mathbb{I}_{\text{contact}}$ denotes contact flag. Finally, we introduce the Foothold Penalty: $r_{\text{foothold}} = r_{\text{toe}} + r_{\text{sole}}$. An illustration of the proposed Foothold Penalty is provided in Figure 8. More reward settings can be found in Section B.3.

5 Experiment

5.1 Experimental Setup

We conduct policy training and deployment on a 28-DoF full-size Kuavo humanoid robot. To evaluate the contribution of key components in our method, we compare our approach (**Ours**) against the following baselines: (1) a RL baseline trained through a vanilla Actor-Critic approach [1] (**Baseline RL**); (2) our method without conditioning the discriminator on the terrain embedding $h_t^{\text{emb}, d}$ (**Ours w/o Condition**); (3) our method without the CVAE module, where expert state transitions are randomly sampled from the expert dataset \mathcal{D} (**Ours w/o CVAE**); and (4) our method without the Foothold Penalty (**Ours w/o Foothold**).

5.2 Motion Style Distribution

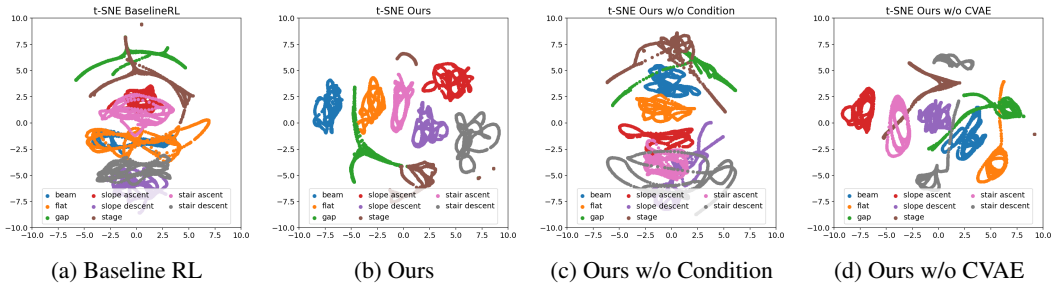


Figure 3: t-SNE visualization of robot joint trajectories across eight terrains. (c) Removing $h_t^{\text{emb}, d}$ significantly weakens the discriminator’s ability to separate different motion styles. (d) The CVAE generates terrain-adaptive style transitions, facilitating efficient policy learning.

To analyze the motion style distributions learned by different methods, we separately perform 700-step rollouts across eight terrains under four policies and collect the robot joint trajectories $\{q_t\}_{t=1}^{700}$ as motion style representations. We then apply t-SNE [45] to all collected trajectories for visual clustering analysis. As shown in Figure 3, the comparison methods exhibit less compact motion distributions with significant inter-terrain overlap. In contrast, our method produces highly compact intra-terrain clusters and clearly separable inter-terrain distributions. Figure 3c shows that introducing terrain-conditioned features improves the discriminator’s ability to separate different motion styles, thereby enhancing terrain-aware motion style regularization. Figure 3d demonstrates that the CVAE-learned terrain-conditioned motion manifold can generate adaptive motion styles across different terrains, facilitating efficient policy learning from diverse motion patterns.

5.3 Performance Comparison

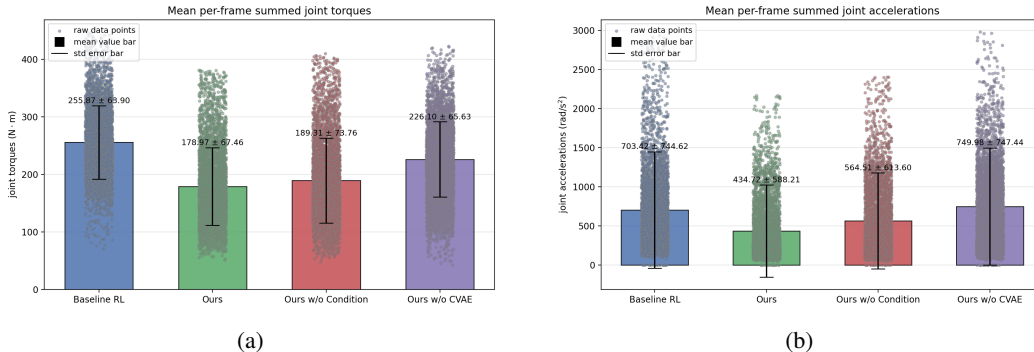


Figure 4: Motion smoothness analysis across all terrains. (a) Mean and standard deviation of joint torques. (b) Mean and standard deviation of joint accelerations.

Motion Smoothness To evaluate locomotion smoothness, we separately perform 700-step roll-outs across eight terrains under four policies and report the mean and standard deviation of whole-body joint torques and joint accelerations. As shown in Figure 4, the proposed method exhibits lower torque and acceleration fluctuations, indicating smoother and more physically coordinated locomotion dynamics. Quantitatively, our method achieves an average whole-body joint torque of 178.97 N · m and joint acceleration of 434.72 rad/s², corresponding to reductions of 30.01% and 38.20% compared to Baseline RL, respectively. This improvement can be attributed to the ability of T-GMP to effectively model terrain-aware anthropomorphic motion patterns from expert data, leading to increased dynamic consistency and reduced joint oscillations.

Table 1: Comparison of success rates for traversing all terrains in a single run.

Method	Success Rate (%)						
	Gap	Beam	Stage	Stair Ascent	Stair Descent	Slope Ascent	Slope Descent
Baseline RL [1]	92.97	79.69	93.36	86.33	85.55	92.19	95.31
Ours	98.83	96.88	96.09	96.48	93.75	99.61	100.00
Ours w/o Condition	96.88	81.41	89.06	96.09	82.42	98.44	97.66
Ours w/o CVAE	97.27	78.52	91.80	91.80	84.38	96.48	97.66
Ours w/o Foothold	98.05	94.14	95.70	95.70	85.94	99.61	98.83

Success Rate We evaluate the terrain traversal success rates of all methods across eight terrains, with detailed experimental settings provided in Section C and results summarized in Table 1. Overall, our proposed method achieves the highest success rates across all tested terrains, demonstrating superior terrain adaptability and locomotion robustness. We attribute this improvement to the effective modeling of terrain-aware anthropomorphic motion priors, which enable coordinated whole-body behaviors that better maintain dynamic balance and improve adaptation to terrain perturbations. In the beam traversal task, our method achieves an average improvement of 17.01% points over the baselines, mainly due to the coordinated arm-extension behaviors for balance regulation. In the downstairs traversal task, our method achieves an average improvement of 9.18% points, benefiting from adaptive center-of-mass lowering and the proposed Foothold Penalty, which suppresses unstable edge contacts and sliding behaviors through reliable foothold control.

5.4 Real-world Deployment

We compare expert demonstrations with real-robot deployments to analyze the consistency of terrain-conditioned motion distributions learned by the policy. Experiments are conducted on the

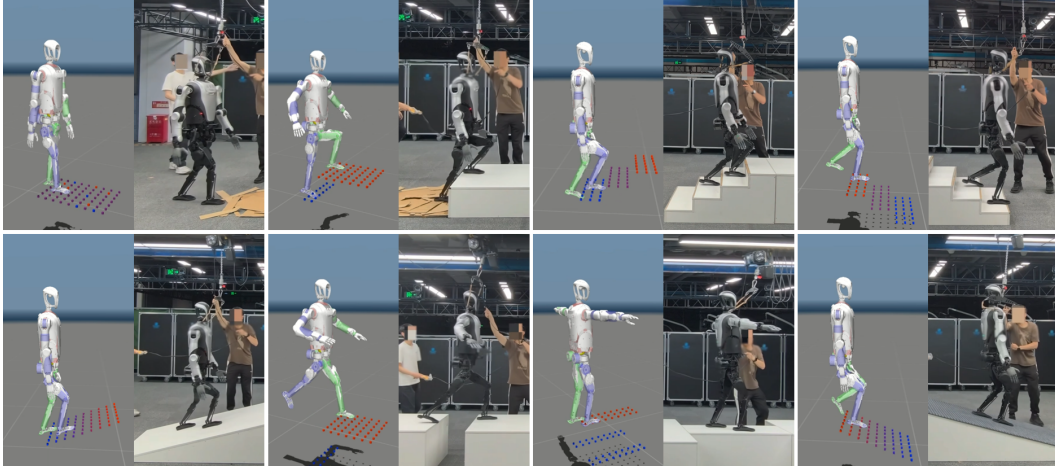


Figure 5: The robot exhibits terrain-adaptive and anthropomorphic locomotion behaviors across diverse terrains, including natural arm swinging during flat-ground walking, lowered center-of-mass postures on stairs and slopes, and arm extension for dynamic balance on gaps and beams.

full-size Kuavo humanoid robot over diverse terrains, including flat ground, a 0.3 m high stage, stairs with 0.13 m step height and 0.28 m tread width, a 15° slope, a 0.4 m wide gap, and a 0.35 m wide beam (with the robot foot separation being 0.3 m). As shown in Figure 5, our method effectively preserves diverse terrain-conditioned expert motion patterns, while exhibiting coordinated and anthropomorphic locomotion behaviors during real-world deployment.

6 Conclusion

In this work, we propose T-GMP, which unifies anthropomorphic naturalness and robust terrain traversal for humanoid locomotion. By leveraging a CVAE, our method successfully learned a generative manifold of human movements that is intrinsically aligned with the terrain-aware physical constraints. Our approach moves beyond static motion priors by employing a terrain-conditioned discriminator that dynamically modulates the naturalness reward, enabling the agent to discover sophisticated balancing strategies, such as reflexive arm-spreading on a narrow beam. Experimental results demonstrate that T-GMP improves traversal success rates and motion smoothness by promoting physically coordinated and anthropomorphic whole-body behaviors across diverse terrains. Our work suggests that integrating generative motion priors conditioned on perceptual observations into RL is a powerful paradigm for achieving the next level of agile and human-like robot locomotion.

7 Limitations and Future Work

First, T-GMP relies on paired motion states and local height maps for training. While privileged policies can conveniently generate synchronized motion and terrain data, the resulting trajectories often lack anthropomorphic naturalness. Although MoCap data provide highly natural human motions, constructing temporally aligned terrain observations remains challenging. Future work may explore adversarial motion regularization during privileged policy training to efficiently generate natural and physically feasible expert trajectories with synchronized terrain observations.

Second, the proposed terrain perception pipeline relies on LiDAR-based environment reconstruction. However, LiDAR measurements inevitably contain sensing noise and reconstruction artifacts. Such perception uncertainties may compromise locomotion robustness on complex terrains. Meanwhile, terrain reconstruction suffers from limited update frequency. Future work may investigate multi-modal perception strategies that integrate depth cameras with LiDAR sensing to improve reconstruction accuracy and perception update frequency.

References

- [1] N. Rudin, D. Hoeller, P. Reist, and M. Hutter. Learning to walk in minutes using massively parallel deep reinforcement learning. In A. Faust, D. Hsu, and G. Neumann, editors, *Proceedings of the 5th Conference on Robot Learning*, volume 164 of *Proceedings of Machine Learning Research*, pages 91–100. PMLR, 08–11 Nov 2022. URL <https://proceedings.mlr.press/v164/rudin22a.html>.
- [2] I. Radosavovic, T. Xiao, B. Zhang, T. Darrell, J. Malik, and K. Sreenath. Real-world humanoid locomotion with reinforcement learning. *Science Robotics*, 9(89):eadi9579, 2024. doi:10.1126/scirobotics.adi9579. URL <https://www.science.org/doi/abs/10.1126/scirobotics.adi9579>.
- [3] Z. Li, X. B. Peng, P. Abbeel, S. Levine, G. Berseth, and K. Sreenath. Reinforcement learning for versatile, dynamic, and robust bipedal locomotion control. *The International Journal of Robotics Research*, 44:840 – 888, 2024. URL <https://api.semanticscholar.org/CorpusID:267320454>.
- [4] Y. Zhou, J. Qiu, W. Zhang, and F. Ni. Humanoidmamba: Generalized mamba-based policy learning with next-action prediction for humanoid locomotion. *IEEE Transactions on Cognitive and Developmental Systems*, pages 1–13, 2026. doi:10.1109/TCDS.2026.3678742.
- [5] D. Hoeller, N. Rudin, D. Sako, and M. Hutter. Anymal parkour: Learning agile navigation for quadrupedal robots. *Science Robotics*, 9(88):eadi7566, 2024. doi:10.1126/scirobotics.adi7566. URL <https://www.science.org/doi/abs/10.1126/scirobotics.adi7566>.
- [6] I. Radosavovic, S. Kamat, T. Darrell, and J. Malik. Learning humanoid locomotion over challenging terrain. *ArXiv*, abs/2410.03654, 2024. URL <https://api.semanticscholar.org/CorpusID:273162639>.
- [7] W. Sun, B. Cao, L. Chen, Y. Su, Y. Liu, Z. Xie, and H. Liu. Learning perceptive humanoid locomotion over challenging terrain. In *2025 IEEE/RSJ International Conference on Intelligent Robots and Systems (IROS)*, pages 6571–6578, 2025. doi:10.1109/IROS60139.2025.11247685.
- [8] Q. Ben, B. Xu, K. Li, F. Jia, W. Zhang, J. Wang, J. Wang, D. Lin, and J. Pang. Gallant: Voxel grid-based humanoid locomotion and local-navigation across 3d constrained terrains. *arXiv preprint arXiv:2511.14625*, 2025.
- [9] X. B. Peng, P. Abbeel, S. Levine, and M. van de Panne. Deepmimic: example-guided deep reinforcement learning of physics-based character skills. *ACM Transactions on Graphics*, 37(4):1–14, July 2018. ISSN 1557-7368. doi:10.1145/3197517.3201311. URL <http://dx.doi.org/10.1145/3197517.3201311>.
- [10] Q. Liao, T. E. Truong, X. Huang, Y. Gao, G. Tevet, K. Sreenath, and C. K. Liu. Beyondmimic: From motion tracking to versatile humanoid control via guided diffusion, 2025. URL <https://arxiv.org/abs/2508.08241>.
- [11] A. Allshire, H. Choi, J. Zhang, D. McAllister, A. Zhang, C. M. Kim, T. Darrell, P. Abbeel, J. Malik, and A. Kanazawa. Visual imitation enables contextual humanoid control. In J. Lim, S. Song, and H.-W. Park, editors, *Proceedings of The 9th Conference on Robot Learning*, volume 305 of *Proceedings of Machine Learning Research*, pages 794–815. PMLR, 27–30 Sep 2025. URL <https://proceedings.mlr.press/v305/allshire25a.html>.
- [12] J. Ni, Z. Wang, W. Lin, A. Bar, Y. LeCun, T. Darrell, J. Malik, and R. Herzig. From generated human videos to physically plausible robot trajectories, 2025. URL <https://arxiv.org/abs/2512.05094>.

- [13] J. Lee, J. Hwangbo, L. Wellhausen, V. Koltun, and M. Hutter. Learning quadrupedal locomotion over challenging terrain. *Science Robotics*, 5(47):eabc5986, 2020. doi: 10.1126/scirobotics.abc5986. URL <https://www.science.org/doi/abs/10.1126/scirobotics.abc5986>.
- [14] A. Kumar, Z. Fu, D. Pathak, and J. Malik. RMA: Rapid Motor Adaptation for Legged Robots. In *Proceedings of Robotics: Science and Systems*, Virtual, July 2021. doi:10.15607/RSS.2021.XVII.011.
- [15] J. Long, Z. Wang, Q. Li, L. Cao, J. Gao, and J. Pang. Hybrid internal model: Learning agile legged locomotion with simulated robot response. In *The Twelfth International Conference on Learning Representations*, 2024. URL <https://openreview.net/forum?id=93LoCyww8o>.
- [16] I. M. Aswin Nahrendra, B. Yu, and H. Myung. Dreamwaq: Learning robust quadrupedal locomotion with implicit terrain imagination via deep reinforcement learning. In *2023 IEEE International Conference on Robotics and Automation (ICRA)*, pages 5078–5084, 2023. doi: 10.1109/ICRA48891.2023.10161144.
- [17] I. Radosavovic, T. Xiao, B. Zhang, T. Darrell, J. Malik, and K. Sreenath. Real-world humanoid locomotion with reinforcement learning. *Science Robotics*, 9(89):ead9579, 2024. doi:10.1126/scirobotics.adi9579. URL <https://www.science.org/doi/abs/10.1126/scirobotics.adi9579>.
- [18] I. M. A. Nahrendra, B. Yu, M. Oh, D. Lee, S. Lee, H. Lee, H. Lim, and H. Myung. Dreamwaq++: Obstacle-aware quadrupedal locomotion with resilient multi-modal reinforcement learning. *IEEE Transactions on Robotics*, pages 1–17, 2026. doi:10.1109/TRO.2026.3653774.
- [19] A. Agarwal, A. Kumar, J. Malik, and D. Pathak. Legged locomotion in challenging terrains using egocentric vision. In K. Liu, D. Kulic, and J. Ichnowski, editors, *Proceedings of The 6th Conference on Robot Learning*, volume 205 of *Proceedings of Machine Learning Research*, pages 403–415. PMLR, 14–18 Dec 2023. URL <https://proceedings.mlr.press/v205/agarwal23a.html>.
- [20] Z. Zhuang, Z. Fu, J. Wang, C. G. Atkeson, S. Schertfeger, C. Finn, and H. Zhao. Robot parkour learning. In J. Tan, M. Toussaint, and K. Darvish, editors, *Proceedings of The 7th Conference on Robot Learning*, volume 229 of *Proceedings of Machine Learning Research*, pages 73–92. PMLR, 06–09 Nov 2023. URL <https://proceedings.mlr.press/v229/zhuang23a.html>.
- [21] Z. Zhuang, S. Yao, and H. Zhao. Humanoid parkour learning. In P. Agrawal, O. Kroemer, and W. Burgard, editors, *Proceedings of The 8th Conference on Robot Learning*, volume 270 of *Proceedings of Machine Learning Research*, pages 1975–1991. PMLR, 06–09 Nov 2025. URL <https://proceedings.mlr.press/v270/zhuang25a.html>.
- [22] S. Zhu, Z. Zhuang, M. Zhao, K.-Y. Lee, and H. Zhao. Hiking in the wild: A scalable perceptive parkour framework for humanoids, 2026. URL <https://arxiv.org/abs/2601.07718>.
- [23] T. Miki, J. Lee, J. Hwangbo, L. Wellhausen, V. Koltun, and M. Hutter. Learning robust perceptive locomotion for quadrupedal robots in the wild. *Science Robotics*, 7(62), Jan. 2022. ISSN 2470-9476. doi:10.1126/scirobotics.abk2822. URL <http://dx.doi.org/10.1126/scirobotics.abk2822>.
- [24] A. Agarwal, A. Kumar, J. Malik, and D. Pathak. Legged locomotion in challenging terrains using egocentric vision. In K. Liu, D. Kulic, and J. Ichnowski, editors, *Proceedings of The 6th Conference on Robot Learning*, volume 205 of *Proceedings of Machine Learning Research*, pages 403–415. PMLR, 14–18 Dec 2023. URL <https://proceedings.mlr.press/v205/agarwal23a.html>.

- [25] X. Cheng, K. Shi, A. Agarwal, and D. Pathak. Extreme parkour with legged robots. *arXiv preprint arXiv:2309.14341*, 2023.
- [26] O. A. V. Magaña, V. Barasuol, M. Camurri, L. Franceschi, M. Focchi, M. Pontil, D. G. Caldwell, and C. Semini. Fast and continuous foothold adaptation for dynamic locomotion through cnns. *IEEE Robotics and Automation Letters*, 4(2):2140–2147, 2019. doi:10.1109/LRA.2019.2899434.
- [27] J. Long, J. Ren, M. Shi, Z. Wang, T. Huang, P. Luo, and J. Pang. Learning humanoid locomotion with perceptive internal model. In *2025 IEEE International Conference on Robotics and Automation (ICRA)*, pages 9997–10003, 2025. doi:10.1109/ICRA55743.2025.11128333.
- [28] H. Wang, Z. Wang, J. Ren, Q. Ben, T. Huang, W. Zhang, and J. Pang. BeamDojo: Learning Agile Humanoid Locomotion on Sparse Footholds. In *Proceedings of Robotics: Science and Systems*, Los Angeles, CA, USA, June 2025. doi:10.15607/RSS.2025.XXI.068.
- [29] F. Jenelten, J. He, F. Farshidian, and M. Hutter. Dtc: Deep tracking control. *Science Robotics*, 9(86):eadh5401, 2024. doi:10.1126/scirobotics.adh5401. URL <https://www.science.org/doi/abs/10.1126/scirobotics.adh5401>.
- [30] J. He, C. Zhang, F. Jenelten, R. Grandia, M. Bächer, and M. Hutter. Attention-based map encoding for learning generalized legged locomotion. *Science Robotics*, 10(105):eadv3604, 2025. doi:10.1126/scirobotics.adv3604. URL <https://www.science.org/doi/abs/10.1126/scirobotics.adv3604>.
- [31] C. Zhang, V. Klemm, F. Yang, and M. Hutter. Ame-2: Agile and generalized legged locomotion via attention-based neural map encoding, 2026. URL <https://arxiv.org/abs/2601.08485>.
- [32] A. Serifi, R. Grandia, E. Knoop, M. Gross, and M. Bächer. Vmp: Versatile motion priors for robustly tracking motion on physical characters. *Computer Graphics Forum*, 43(8):e15175, 2024. doi:<https://doi.org/10.1111/cgf.15175>. URL <https://onlinelibrary.wiley.com/doi/abs/10.1111/cgf.15175>.
- [33] Y. Ze, S. Zhao, W. Wang, A. Kanazawa, R. Duan, P. Abbeel, G. Shi, J. Wu, and C. K. Liu. Twist2: Scalable, portable, and holistic humanoid data collection system, 2025. URL <https://arxiv.org/abs/2511.02832>.
- [34] X. B. Peng, Z. Ma, P. Abbeel, S. Levine, and A. Kanazawa. Amp: Adversarial motion priors for stylized physics-based character control. *ACM Trans. Graph.*, 40(4), July 2021. doi:10.1145/3450626.3459670. URL <http://doi.acm.org/10.1145/3450626.3459670>.
- [35] X. B. Peng, Y. Guo, L. Halper, S. Levine, and S. Fidler. Ase: Large-scale reusable adversarial skill embeddings for physically simulated characters. *ACM Trans. Graph.*, 41(4), July 2022.
- [36] Z. Dou, X. Chen, Q. Fan, T. Komura, and W. Wang. C-ase: Learning conditional adversarial skill embeddings for physics-based characters. In *SIGGRAPH Asia 2023 Conference Papers*, SA '23, New York, NY, USA, 2023. Association for Computing Machinery. ISBN 9798400703157. doi:10.1145/3610548.3618205. URL <https://doi.org/10.1145/3610548.3618205>.
- [37] H. Wang, W. Zhang, R. Yu, T. Huang, J. Ren, F. Jia, Z. Wang, X. Niu, X. Chen, J. Chen, Q. Chen, J. Wang, and J. Pang. Physhsi: Towards a real-world generalizable and natural humanoid-scene interaction system. *ArXiv*, abs/2510.11072, 2025. URL <https://api.semanticscholar.org/CorpusID:282057062>.
- [38] J. Wang, Y. Jiang, H. Zhang, C. Tessler, D. Rempe, J. Hodgins, and X. B. Peng. Hil: Hybrid imitation learning of diverse parkour skills from videos. *ArXiv*, abs/2505.12619, 2025. URL <https://api.semanticscholar.org/CorpusID:278741010>.

- [39] H. Zhang, L. Zhang, Z. Chen, L. Chen, Y. Wang, and R. Xiong. Natural humanoid robot locomotion with generative motion prior. In *2025 IEEE/RSJ International Conference on Intelligent Robots and Systems (IROS)*, pages 6622–6629, 2025. doi:10.1109/IROS60139.2025.11247682.
- [40] Q. Li, C. Zhu, Y. Wu, X. Yuan, Z. Zhang, J. Yang, and Y. Liu. Run: Residual policy for natural humanoid locomotion. *ArXiv*, abs/2509.20696, 2025. URL <https://api.semanticscholar.org/CorpusID:281526091>.
- [41] Y. Fan, T. Gui, K. Ji, S. Ding, C. Zhang, J. Gu, J. Yu, J. Wang, and Y. Shi. One policy but many worlds: A scalable unified policy for versatile humanoid locomotion, 2025. URL <https://arxiv.org/abs/2505.18780>.
- [42] Z. Zhang, K. Wen, M. Xu, J. He, C. Li, T. Miki, C. Schwarke, C. Zhang, X. B. Peng, and M. Hutter. Learning whole-body humanoid locomotion via motion generation and motion tracking, 2026. URL <https://arxiv.org/abs/2604.17335>.
- [43] J. P. Araujo, Y. Ze, P. Xu, J. Wu, and C. K. Liu. Retargeting matters: General motion retargeting for humanoid motion tracking, 2025. URL <https://arxiv.org/abs/2510.02252>.
- [44] I. Higgins, L. Matthey, A. Pal, C. Burgess, X. Glorot, M. Botvinick, S. Mohamed, and A. Lerchner. beta-VAE: Learning basic visual concepts with a constrained variational framework. In *International Conference on Learning Representations*, 2017. URL <https://openreview.net/forum?id=Sy2fzU9gl>.
- [45] L. van der Maaten and G. Hinton. Visualizing data using t-sne. *Journal of Machine Learning Research*, 9(86):2579–2605, 2008. URL <http://jmlr.org/papers/v9/vandermaaten08a.html>.
- [46] J. Schulman, F. Wolski, P. Dhariwal, A. Radford, and O. Klimov. Proximal policy optimization algorithms, 2017. URL <https://arxiv.org/abs/1707.06347>.
- [47] NVIDIA, :, M. Mittal, P. Roth, J. Tigue, A. Richard, O. Zhang, P. Du, A. Serrano-Muñoz, X. Yao, R. Zurbrügg, N. Rudin, L. Wawrzyniak, M. Rakhsha, A. Denzler, E. Heiden, A. Borovicka, O. Ahmed, I. Akinola, A. Anwar, M. T. Carlson, J. Y. Feng, A. Garg, R. Gasoto, L. Gulich, Y. Guo, M. Gussert, A. Hansen, M. Kulkarni, C. Li, W. Liu, V. Makoviychuk, G. Malczyk, H. Mazhar, M. Moghani, A. Murali, M. Noseworthy, A. Poddubny, N. Ratliff, W. Rehberg, C. Schwarke, R. Singh, J. L. Smith, B. Tang, R. Thaker, M. Trepte, K. V. Wyk, F. Yu, A. Millane, V. Ramasamy, R. Steiner, S. Subramanian, C. Volk, C. Chen, N. Jawale, A. V. Kuruttukulam, M. A. Lin, A. Mandlekar, K. Patzwaldt, J. Welsh, H. Zhao, F. Anes, J.-F. Lafleche, N. Moënné-Loccoz, S. Park, R. Stepinski, D. V. Gelder, C. Amevor, J. Carius, J. Chang, A. H. Chen, P. de Heras Ciechowski, G. Daviet, M. Mohajerani, J. von Muralt, V. Reutsky, M. Sauter, S. Schirm, E. L. Shi, P. Terdiman, K. Vilella, T. Widmer, G. Yeoman, T. Chen, S. Grizan, C. Li, L. Li, C. Smith, R. Wiltz, K. Alexis, Y. Chang, D. Chu, L. J. Fan, F. Farshidian, A. Handa, S. Huang, M. Hutter, Y. Narang, S. Pouya, S. Sheng, Y. Zhu, M. Macklin, A. Moravanszky, P. Reist, Y. Guo, D. Hoeller, and G. State. Isaac lab: A gpu-accelerated simulation framework for multi-modal robot learning, 2025. URL <https://arxiv.org/abs/2511.04831>.
- [48] T. Miki, L. Wellhausen, R. Grandia, F. Jenelten, T. Homberger, and M. Hutter. Elevation mapping for locomotion and navigation using gpu, 2022. URL <https://arxiv.org/abs/2204.12876>.

A Data Collection

A.1 Privileged Policy Training

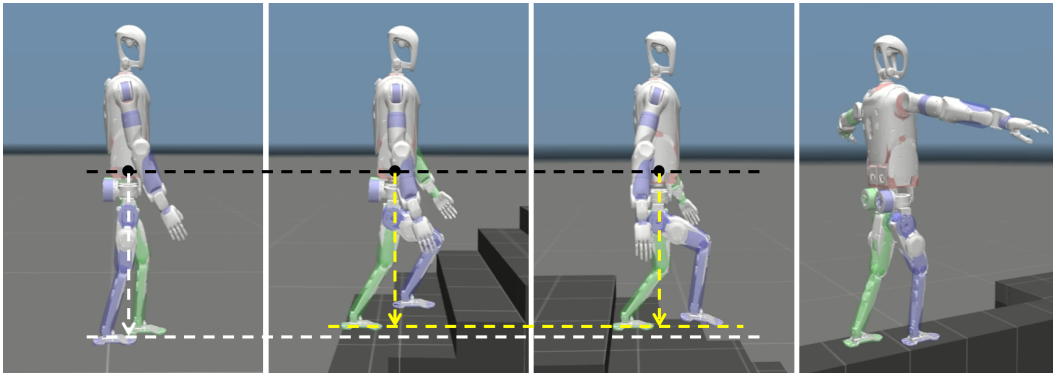


Figure 6: For challenging terrains such as stairs and beams, we introduce terrain-specific constraints on center-of-mass regulation and arm-balancing behaviors through reward design to promote more anthropomorphic and robust whole-body locomotion.

To obtain high-quality expert motion data, we train privileged policies on challenging terrains, including stages, slopes, and beams, to generate physically feasible and terrain-adaptive reference trajectories. Specifically, privileged observations and exteroceptive observations are incorporated during training to explicitly integrate high-dimensional terrain-aware features. Privileged observations provide richer state information for more stable and precise locomotion control, while exteroceptive observations enable the policy to perceive local terrain variations and improve foresighted adaptation of foothold placement and motion behaviors. In particular, as shown in Figure 6, for stairs and slopes, we design terrain-specific rewards that encourage lowering the robot’s center of mass to improve locomotion stability on challenging terrains. For beam traversal, we further design anthropomorphic arm-balancing behaviors to enhance dynamic balance stability in narrow support regions. Detailed configurations of privileged observations are provided in Table 2.

A.2 Data Utilization Efficiency

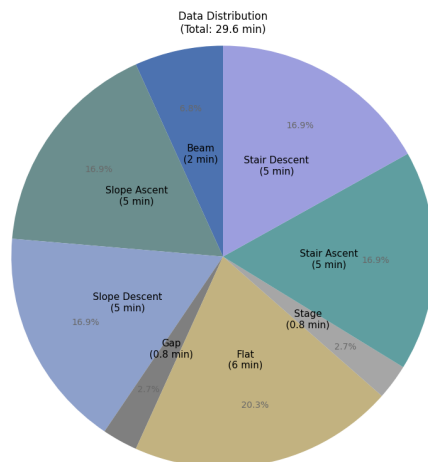


Figure 7: Distribution of motion data across eight terrains. Motion trajectories collected using privileged policies on challenging terrains contain 1000 frames each and cover terrain configurations with varying difficulty levels (e.g., beams with widths of 0.3 m, 0.35 m, and 0.4 m). Data generated using GMR consists of fixed-length trajectories of 400 frames and includes diverse locomotion behaviors (e.g., straight walking and turning motions on flat ground).

Benefiting from the proposed T-GMP, we learn a terrain-conditioned motion manifold spanning eight terrains using only approximately 29.6 min (88.8k frames) of data. As shown in Figure 7, the proposed method effectively captures diverse anthropomorphic locomotion patterns from limited expert demonstrations while covering diverse terrain conditions, locomotion behaviors, and difficulty distributions, demonstrating strong data efficiency and motion generalization capabilities.

B Policy Training

B.1 Observations

Table 2: Observation Terms

Term	Notation	Type	Description
Velocity command	c_t	Command	Velocity command of the robot’s base frame
Height scan	h_t	Perception	A 9×7 height scan in front of the robot
Base angular velocity	ω_t	Policy	Angular velocity in the robot’s base frame
Projected gravity	\mathbf{g}_t	Policy	Gravity projection on the robot’s base frame
Joint position	q_t	Policy	The joint positions of the robot
Joint velocity	\dot{q}_t	Policy	The joint velocities of the robot
Last action	a_{t-1}	Policy	The last input action to the environment
Base linear velocity	v_t	Privilege	Linear velocity in the robot’s base frame
Joint torque	τ_t	Privilege	Torques applied to the robot’s joint
Joint acceleration	\ddot{q}_t	Privilege	The joint accelerations of the robot
Feet linear velocity	v_t^{feet}	Privilege	The linear velocity of the robot’s feet
Feet contact force	F_t^{contact}	Privilege	Contact force on the robot’s feet
Mass	m	Privilege	Total mass of the robot
Material	μ	Privilege	Friction coefficient of the ground
Center of mass	p_{com}	Privilege	Center of mass in the robot’s base frame
Action delay	t_{delay}	Privilege	Action delay on the robot’s motors
Push force	F_t^{ext}	Privilege	External push force applied on the robot
Push torque	τ_t^{ext}	Privilege	External push torque applied on the robot
Feet height	h_t^{feet}	Privilege	Robot’s feet height
Feet air time	t_{air}	Privilege	Robot’s feet air time since last contact

Table 2 summarizes all observations used by the Actor and Critic. The Actor inputs consist of command observations, perceptual observations, and policy observations, enabling the policy to jointly capture robot dynamics and local terrain geometry. Specifically, the velocity command c_t consists of linear and angular velocity commands, i.e., $c_t = [v_t, \omega_t]$. To improve value estimation accuracy, we introduce privileged observations that are unavailable during real-world deployment into the Critic network during training. These privileged observations are only used to facilitate more accurate value learning for the Critic and are not provided to the Actor during policy execution, thereby ensuring deployment compatibility and perception consistency under real-world conditions.

B.2 Reinforcement Learning Setup

Policy optimization is performed using Proximal Policy Optimization (PPO) [46], with the associated training hyperparameters summarized in Table 3. All experiments are conducted in the Isaac Lab [47] simulation environment on a single NVIDIA RTX 4090 GPU, with 2,048 environments running in parallel. We adopt an asymmetric Actor-Critic architecture to train the policy, where both the Actor and Critic are parameterized by multilayer perceptrons (MLPs) with hidden layer sizes of [512, 256, 128].

Table 3: PPO Hyperparameters

Parameter	Value
Batch size	$24 \cdot 2048 = 49152$
Mini batch size	$6 \cdot 2048 = 12288$
Number of epochs	5
Clip range	0.2
Entropy coefficient	0.005
Discount factor	0.99
GAE discount factor	0.95
Desired KL-divergence	0.01
Learning rate	0.001
Max gradient norm	1.0

B.3 Reward Formulation

Table 4: Reward Terms

Term	Function	Weight
Linear velocity command tracking	$\exp(\ v_{xy} - v_{xy}^{\text{cmd}}\ ^2)$	5.0
Angular velocity command tracking	$\exp(\ \omega_z - \omega_z^{\text{cmd}}\ ^2)$	3.0
Joint velocity	$\ \dot{q}\ ^2$	-2.0×10^{-3}
Joint acceleration	$\ \ddot{q}\ ^2$	-2.5×10^{-7}
Joint torque	$\ \tau\ ^2$	-1.0×10^{-5}
Joint power	$ \tau \cdot \dot{q} $	-2.0×10^{-5}
Action rate	$\ a_t - a_{t-1}\ ^2$	-0.005
Action smoothness	$\ (a_t - a_{t-1}) - (a_{t-1} - a_{t-2})\ ^2$	-0.01
Joint limit	$\max(0, q - q_{\max}) + \max(0, q_{\min} - q)$	-1.0
Feet slide	$\ v_{xy}^{\text{feet}}\ _2^2 * \mathbb{I}_{\text{contact}}$	-0.1
Contact force	$\max(0, f_{\text{contact}} - f_{\text{threshold}})$	-0.001
Termination	$\mathbb{I}_{\text{reset}}$	-200

Since motion style is primarily guided by the discriminator, the reward design remains concise yet effective. The reward received by the policy during training consists of four components: (1) task reward r_{task} , which encourages the robot’s root to track the commanded linear and angular velocities, (2) regularization reward r_{reg} , which enforces smoothness in actions and states while ensuring physical plausibility, (3) style reward r_{amp} , provided by the style discriminator, which encourages policy-induced state transitions to align with the expert motion styles, and (4) foothold penalty r_{foothold} , which penalizes undesirable foot-contact behaviors. The overall training reward is defined as:

$$r = w_1 r_{\text{task}} + w_2 r_{\text{reg}} + w_3 r_{\text{amp}} + w_4 r_{\text{foothold}}, \quad (9)$$

where w_i represents the corresponding weights.

Benefiting from the inclusion of the style reward, the policy becomes significantly less sensitive to reward weighting, leading to a more stable and efficient hyperparameter tuning process. In practice, a single set of reward parameters can be reused across subsequent training runs with only minimal adjustment. We design a unified and concise reward function to train all policies. We primarily focus on the smoothness of robot motion and energy consumption, enabling the reward function to remain consistent across different tasks and experimental settings, thereby avoiding additional task-

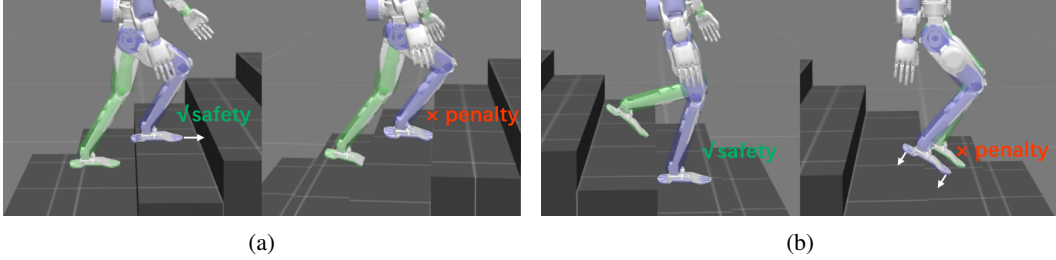


Figure 8: Illustration of the Foothold Penalty mechanism. (a) During stair ascent, the minimum toe-terrain contact distance d_{toe} is evaluated to reduce potential toe-collision risks. (b) During stair descent, the maximum sole-terrain contact distance d_{sole} is evaluated to suppress unstable foothold behaviors such as edge contacts and slipping.

or scenario-specific reward engineering. The definitions of all reward terms and their corresponding weights are summarized in Table 4.

B.4 Foothold Penalty

We design a Foothold Penalty mechanism to explicitly regularize the contact quality between the robot feet and the terrain. As illustrated in Figure 8a, during terrain traversal, we compute the minimum distance d_{toe} between the toe and the terrain surface. A penalty is applied when the distance exceeds the threshold $d_{\text{toe}}^{\text{threshold}}$, suppressing potential toe-collision behaviors. Meanwhile, as illustrated in Figure 8b, we further compute the maximum distance d_{sole} between the sole and the terrain surface. When the distance exceeds the threshold $d_{\text{sole}}^{\text{threshold}}$, an additional penalty is imposed to discourage unstable support behaviors such as edge contacts and slipping. This mechanism encourages the policy to learn more stable and physically feasible foothold patterns, thereby improving locomotion stability and traversal robustness on complex terrains.

C Success Rate Configurations

We evaluate terrain traversal success rates on eight representative challenging terrains, including a 0.3 m high stage, stairs with 0.13 m step height and 0.28 m tread width, a 15° slope, a 0.4 m wide gap, and a 0.35 m wide beam. Each terrain is constructed within an $8\text{ m} \times 8\text{ m}$ evaluation area. A trial is considered successful if the robot completes a full terrain traversal within a predefined time limit. Failure is recorded if any body part other than the feet collides with the terrain during traversal, any joint exceeds its position limits or exhibits excessively large accelerations, or if the robot fails to complete the traversal within the allotted time.

D Sim-to-Real Details

D.1 Robot Setup

The full-size Kuavo humanoid robot is 1.66 m tall, weighs approximately 55 kg, and possesses 28 Degrees of Freedom (DoFs), including 2 DoFs in the head, 14 DoFs in the arms, and 12 DoFs in the legs. A Mid-360 LiDAR is mounted on the robot head for point-cloud perception and terrain reconstruction. The system adopts a dual-computing architecture, where an Orin-NX module processes point-cloud perception data in real time, while a MoFang i9-13900 computer executes low-level whole-body locomotion control.

The robot is controlled using a joint-space PD controller with control torques defined as:

$$\tau = K_p(q^* - q) - K_d\dot{q}, \quad (10)$$

where K_p and K_d denote proportional and derivative gains, respectively, q denotes the current joint position, and \dot{q} denotes the current joint velocity. The policy action a is defined as a residual control

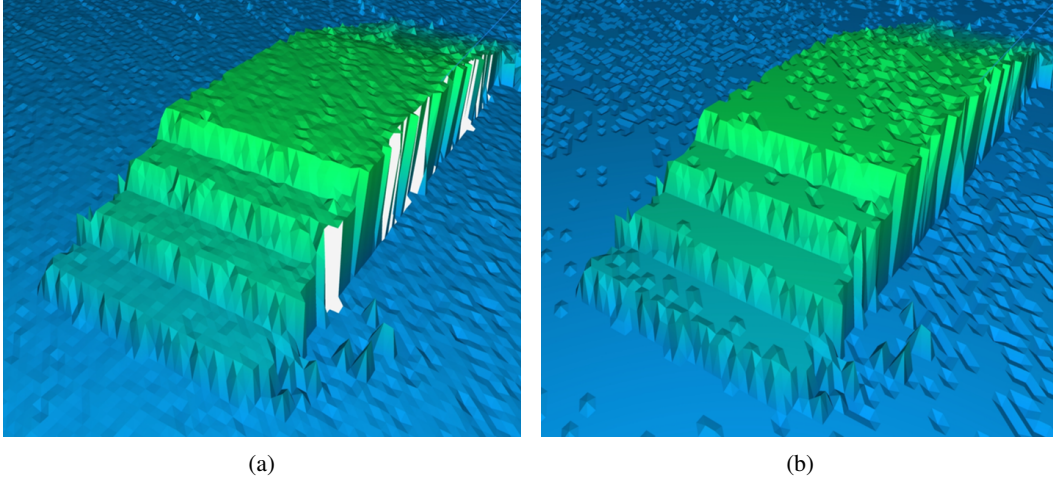


Figure 9: Elevation map construction pipeline. (a) Raw dense elevation map generated from sparse environmental point clouds, containing missing regions caused by incomplete point-cloud reconstruction. (b) Processed elevation map after applying the nearest-region filling strategy, which is used for subsequent height-map sampling.

signal relative to the default joint configuration q_0 , such that the target joint position is given by

$$q^* = q_0 + a. \quad (11)$$

D.2 Acquisition of Elevation Map

As illustrated in Figure 9a, following the elevation mapping pipeline in [48], the raw point cloud observations are converted into a dense elevation map representation. To avoid invalid NaN inputs caused by sparse point-cloud reconstruction, we apply a nearest-region filling strategy that replaces NaN cells with the minimum height value within the surrounding 5×5 neighborhood, resulting in the processed elevation map shown in Figure 9b. We then uniformly sample a local terrain patch of size $0.8 \text{ m} \times 0.6 \text{ m}$ in front of the robot from the processed elevation map, which is used as the terrain perception input to the policy.